A Fast Source Reconstruction Method for Radiating Structures on Large Scattering Platforms

Oscar Borries, Martin Haulund Gæde, Andreas Ericsson,
Peter Meincke and Erik Jørgensen
TICRA
Landemærket 29, 1119 Copenhagen, Denmark
{ob,mhg,ae,pme,ej}@ticra.com

Dennis Schobert and Erio Gandini
ESA-ESTEC
Keplerlaan 1, 2201 AZ Noordwijk, The Netherlands

***Abstract*—We present a fast source reconstruction method suitable for antenna diagnostic applications of radiating structures on electrically large platforms. The method is based on a novel implementation of a recent reformulation of the inverse electromagnetic scattering problem, and is solved using a Higher Order Method of Moments (MoM) discretization. The novel implementation achieves asymptotically better scaling than previously possible, and in particular the memory use is substantially lower than was previously possible. Results from two example cases are presented where the new method is compared to the current commercial state-of-the-art solver in DIATOOL 1.1, and significant improvements are observed in terms of computation times and memory requirements.**

I. Introduction

Source reconstruction is a highly relevant topic that has attracted much attention throughout the past decades in applications such as antenna diagnostics [1]–[3], near-field to far-field transformation and filtering [4], [5], antenna placement investigations [6] and performance analyses of 5G devices [7]. While the applications vary, the fundamental challenge is to find the currents that radiate a specific electromagnetic field.

The electromagnetic source reconstruction problem is a linear inverse problem based on finding currents with known location that radiate a given complex vector field [8]. The problem is naturally formulated in terms of integral equations based directly on Maxwell's equations. For applications with diagnostics purposes, the equations should be augmented with Love's condition of zero fields inside a surface enclosing the sources, such that the sought currents provide a unique solution [9] that represents the actual physical currents on the structure.

Inverse equivalent surface current solvers is the tool that is used to process near-field or far-field measurement data in order to reconstruct the fields or currents in the extreme near-field region of the radiating structure. A common limitation with most inverse equivalent surface current solvers to date is that their computational requirements have less desirable scaling properties in comparison to their forward-solver (radiation problem) counter-parts in terms of frequency, electrical size of the scatterer and the amount of input data required to solve the problem. Much work have been presented to date that attempts to mitigate these limitations [10]–[12], but for diagnostics purposes, the fundamental challenges regarding the required memory and computation time have remained.

In this work, we present the results of a current collaboration between TICRA and the European Space Agency (ESA) in the activity "Fast Diagnostic Methods for Large-Scale Full-Satellite Antenna Measurements", No. AO/1-9352/18/NL/AF. The heritage of TICRA in terms of a state-of-the-art method of moments (MoM) solver, based on higher-order basis functions and higher-order mesh elements [13], together with innovative regularization techniques [14], have been used as a stepping stone to accelerate the development of new improved source reconstruction methods.

The main driver for the improved results in this paper, however, is that of a projection operator based on Calderón operators as first presented in [15]. It has been shown that by using a Calderón projection it is assessed that the achieved solution yields the correct currents from a physical point of view. However, the numerical implementation described in [15] can be improved substantially upon, in particular in terms of the projection operation itself.

In order to achieve acceptable performance when reconstructing currents on electrically large structures, matrix-free representations of the relevant operators are necessary. Using matrix-free operators lead to a number of challenges, in particular regarding the memory/computational time trade-off. The specific implementation shown in this paper achieves drastic improvements, around two orders of magnitude, in terms of memory requirements and computational time, without sacrificing solution accuracy compared to previously presented inverse source reconstruction methods.

The paper is organised as follows, in Section II the theory of the proposed method is presented and in Section III an overview is given of the numerical implementation of the source reconstruction solver. After that, the results from two source reconstruction application cases are presented in Section IV, followed by some concluding remarks in Section V.

II. Theory

The basic electromagnetic concept involved in reconstructing currents is the equivalence principle, which states that the sources and scatterers enclosed inside a reconstruction surface (RS) S, here labelled $\boldsymbol{M}^{\mathrm{int}}$, $\boldsymbol{J}^{\mathrm{int}}$, can be replaced by an equivalent set of surface current densities $\boldsymbol{M}_S, \boldsymbol{J}_S$ on S, such

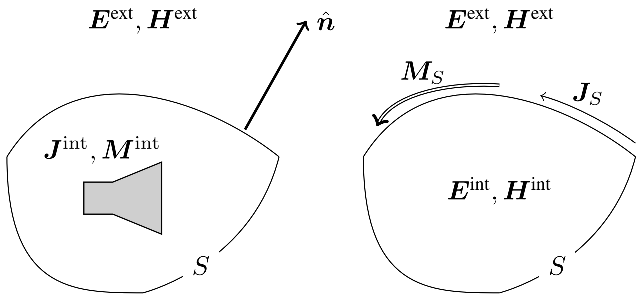

(a) (b)

Fig. 1: The equivalence principle for an imaginary closed surface S: original problem (a) and equivalent problem (b). Introducing surface current densities on S, $\boldsymbol{J}_S$ and $\boldsymbol{M}_S$, which radiate the fields $\boldsymbol{E}^{\text{ext}}$ and $\boldsymbol{H}^{\text{ext}}$ outside S such that the sources inside S can be removed.

that these currents radiate the same fields $\boldsymbol{E}^{\text{ext}}, \boldsymbol{H}^{\text{ext}}$ outside the surface. This concept is illustrated in Fig. 1.

Consequently, $\boldsymbol{E}^{\text{ext}}, \boldsymbol{H}^{\text{ext}}$ and the currents on the surface are related by the outward unit normal vector $\hat{\boldsymbol{n}}$ [16]

$$\boldsymbol{J}_S = \hat{\boldsymbol{n}} \times (\boldsymbol{H}^{\text{ext}} - \boldsymbol{H}^{\text{int}}), \tag{1}$$

$$\boldsymbol{M}_S = -\hat{\boldsymbol{n}} \times (\boldsymbol{E}^{\text{ext}} - \boldsymbol{E}^{\text{int}}). \tag{2}$$

Based on these surface current densities, a data equation can be set up, linking measurements and the equivalent currents [3]

$$\boldsymbol{E}^{\text{meas}}(\boldsymbol{R}) = -j\omega\mu_o \mathcal{L}\boldsymbol{J}_S + \mathcal{K}\boldsymbol{M}_S, \tag{3}$$

where $\boldsymbol{R}$ indicates the observation point, and the integral operators $\mathcal{L}$ and $\mathcal{K}$ are defined in [3, Eq. (3)] as

$$\begin{aligned} \mathcal{L}\boldsymbol{J}_S = &\int_S \boldsymbol{J}_S(\boldsymbol{R}')G(\boldsymbol{R}, \boldsymbol{R}')dS' \\ &+ \frac{1}{k_0^2}\int_S \nabla'_S \cdot \boldsymbol{J}_S(\boldsymbol{R}')\nabla G(\boldsymbol{R}, \boldsymbol{R}')dS' \end{aligned} \tag{4}$$

$$\mathcal{K}\boldsymbol{M}_S = \int_S \boldsymbol{M}_S(\boldsymbol{R}') \times \nabla G(\boldsymbol{R}, \boldsymbol{R}')dS', \tag{5}$$

where $e^{-j\omega t}$ time dependence is assumed and suppressed. In (4), $\boldsymbol{R}'$ denotes the integration point, $k_0 = 2\pi/\lambda_0$ is the free-space wavenumber, λ_0 is the free-space wavelength and $G(\boldsymbol{R}, \boldsymbol{R}') = \exp\left(-jk_0\|\boldsymbol{R} - \boldsymbol{R}'\|_2\right) / \left(4\pi\|\boldsymbol{R} - \boldsymbol{R}'\|_2\right)$ is the scalar Green's function.

The key challenge is that the currents determined by a solution to (3) are non-unique due to the presence of the $-\boldsymbol{H}^{\text{int}}$ and $-\boldsymbol{E}^{\text{int}}$ terms in (1). To overcome this problem Love's equivalent current condition [9] of zero fields inside of S ($\boldsymbol{H}^{\text{int}} = \boldsymbol{E}^{\text{int}} = 0$) is considered

$$\left.\begin{aligned} -\left(\hat{\boldsymbol{n}} \times \mathcal{K} + \tfrac{1}{2}\right)\boldsymbol{J}_S - j\omega\epsilon_o \hat{\boldsymbol{n}} \times \mathcal{L}\boldsymbol{M}_S = 0 \\ -j\omega\mu_o \hat{\boldsymbol{n}} \times \mathcal{L}\boldsymbol{J}_S + \left(\hat{\boldsymbol{n}} \times \mathcal{K} + \tfrac{1}{2}\right)\boldsymbol{M}_S = 0 \end{aligned}\right\} \begin{array}{c}\text{for} \\ \boldsymbol{R} \to S^-. \end{array} \tag{6}$$

This relation enforces the zero-field condition when moving the observation point onto S from the inside. Most previous works are based on solving the coupled system of equations in (3) and (6). However, this approach is computationally expensive to solve in general, and since regularization is needed to balance the two conditions, a matrix-free approach is inefficient.

An alternative approach was suggested recently in [15], where a Calderón projection is used to restrict the solution space to the space spanned by the Love currents. More specifically, a Calderón pre-conditioner was formulated for the iterative solution of the inverse problem. This approach implies that we can find the unique Love currents by starting with any set of the non-unique currents (1), and then simply compute and subtract the contribution from the unwanted interior fields.

$$\left.\begin{aligned} \boldsymbol{J}_S^{\text{Love}} = \left(\hat{\boldsymbol{n}} \times \mathcal{K} - \tfrac{1}{2}\right)\boldsymbol{J}_S + j\omega\epsilon_o \hat{\boldsymbol{n}} \times \mathcal{L}\boldsymbol{M}_S \\ \boldsymbol{M}_S^{\text{Love}} = j\omega\mu_o \hat{\boldsymbol{n}} \times \mathcal{L}\boldsymbol{J}_S - \left(\hat{\boldsymbol{n}} \times \mathcal{K} - \tfrac{1}{2}\right)\boldsymbol{M}_S \end{aligned}\right\} \begin{array}{c}\text{for} \\ \boldsymbol{R} \to S^-. \end{array} \tag{7}$$

The right-hand-side of (7) differ from (6) only through the signs of the various terms. This reflects that the task involves the computation of the interior fields, which may then be forced to zero as in (6) or be used to subtract the unwanted contribution and obtain the Love's currents as in (7). Although the non-uniqueness is solved either by enforcing (6) or by applying the mapping (7), the problem is still ill-posed. A regularization scheme is therefore needed to obtained a stable solution.

III. Implementation

In order to solve the inverse problem numerically, using a simulated or measured field in amplitude and phase as input, the reconstruction surface and the unknown currents are discretized. This implies that the data equation (3) is discretized to a linear system of equations

$$\bar{\bar{A}}\bar{x} = \bar{b}, \tag{8}$$

where $\bar{\bar{A}}$ is a matrix representing the radiation from the unknown currents $\bar{x}$ on S that generate the measured fields in $\bar{b}$. The boundary condition equation (6) is discretized to

$$\bar{\bar{L}}\bar{x} = 0, \tag{9}$$

here $\bar{\bar{L}}$ is the matrix representation of Love's condition. Similarly, the Calderón projection in (7) is discretized to

$$\bar{\bar{P}}\bar{x}^{\text{Love}} = \bar{\bar{C}}\bar{x}, \tag{10}$$

where $\bar{\bar{P}}$ is a sparse projection operator, $\bar{x}$ are the initial reconstructed currents, $\bar{x}^{\text{Love}}$ are the sought after currents that fulfil Love's condition, and $\bar{\bar{C}}$ is similar to $\bar{\bar{L}}$ except for the signs. The discrete form of the Calderón mapping in (10) can be restated as

$$\bar{x}^{\text{Love}} = \bar{\bar{P}}^{-1}\bar{\bar{C}}\bar{x} = \bar{\bar{T}}\bar{x} \tag{11}$$

implying that $\bar{\bar{T}}$ can be seen as a projection operator from the general space of all currents on the RS to the space of currents that fulfil Love's condition.

The mathematical problem to solve can be formulated as

$$\min_{\bar{x}} \|\bar{\bar{A}}\bar{x} - \bar{b}\|_2, \tag{12}$$

$$\text{s.t. } \bar{\bar{L}}\bar{x} = 0, \tag{13}$$

and with the assumption that $\bar{\bar{L}}\bar{\bar{T}}\bar{x} = 0$, i.e. the range of $\bar{\bar{T}}$ coincides with the null-space of $\bar{\bar{L}}$, the Calderón mapping allows us to restate this problem simply as a preconditioned Least Squares problem

$$\min_{\bar{z}} \|\bar{\bar{A}}\bar{\bar{T}}\bar{z} - \bar{b}\|_2, \tag{14}$$

yielding the solution $\bar{x} = \bar{\bar{T}}\bar{z}$. The problem (14) can be solved in a number of ways, and in this work a novel solution procedure is proposed.

The solution procedure consists of using the Conjugate Gradient Least Squares (CGLS) method as an iterative procedure to solve the system $\|\bar{\bar{A}}\bar{x} - \bar{b}\|_2$, and then applying $\bar{\bar{T}}$ to that solution to make sure the solution fulfils Love's condition. After the $\bar{\bar{T}}$ projection, a few additional CGLS iterations are taken to slightly reduce the residual of the system. Specifically, the procedure has three steps:

1) Solve $\bar{y} = \arg\min_{\bar{x}} \|\bar{\bar{A}}\bar{x} - \bar{b}\|_2$ using CGLS.
2) Compute $\bar{z} = \bar{\bar{T}}\bar{y}$.
3) Take a few iterations of CGLS applied to the problem $\bar{y} = \arg\min_{\bar{x}} \|\bar{\bar{A}}\bar{x} - \bar{b}\|_2$, with starting guess $\bar{x}_0 = \bar{z}$.

This procedure has several advantages. First and foremost, only one matrix-vector product with $\bar{\bar{T}}$ is necessary which means that $\bar{\bar{T}}$ does not need to be stored. Second, the only matrix needed to be inverted is $\bar{\bar{P}}$. This matrix is extremely well conditioned, and since it is only needed once during the application of $\bar{\bar{T}}$, the action of inverse can be computed using an iterative solver. Finally, the only matrix to be applied multiple times is $\bar{\bar{A}}$, and many efficient algorithms exist for computing the action of this matrix and its hermitian. Crucially, all matrix multiplications with $\bar{\bar{A}}$, $\bar{\bar{A}}^H$ and $\bar{\bar{C}}$ are done using so-called fast methods, i.e. methods that scale at most as $\mathcal{O}(a \log b)$ where $a = b = \max\{M, N\}$, and $M/2$ is the number of measurement data points and N is the number of unknowns. Since $\bar{\bar{P}}$ is generated on-the-fly and is sparse with $\mathcal{O}(N)$ elements, this means that both memory and computational time scales as $\mathcal{O}(N \log N)$ or $\mathcal{O}(M \log M)$, which is asymptotically better than all previously published methods.

IV. Results

Two application cases are presented where the proposed source reconstruction solver is put to the test. The first case consists of simulated data of a 10 GHz reflector antenna on a satellite platform. There are a number of advantages associated with using simulated data as input to the source reconstruction software. For example, noise can easily be added manually to the data to synthesise any level of measurement noise, and the errors in the reconstructed fields and currents can be computed from comparison with known near-field data. This case will test if the presented method can handle source reconstruction of extremely large problems. The second case consists of measured data of a 664 GHz feed horn from the meteorological operational satellite second generation (MetOp-SG) ice cloud imager in [17]. This case will test how well suited the presented method is for high frequency source reconstruction applications.

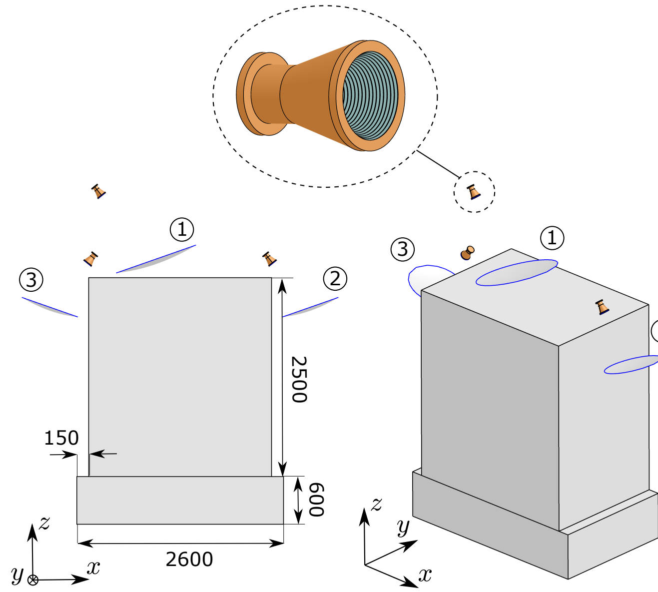

Fig. 2: Application case 1, OHB SmallGeo satellite platform with three reflector antennas illuminated by corrugated feed horns, seen from two different perspectives.

A. Reflector antenna on satellite platform

A simplified model of the OHB SmallGeo satellite platform with three reflector antennas was implemented in TICRA Tools. The platform has the outer dimensions 2.6 m x 1.6 m x 3.1 m and is presented in Fig. 2. The reflectors, which are labelled 1, 2 and 3 in Fig. 2, are each illuminated by a corrugated horn antenna, located at the reflector focal point, operating at 10 GHz with an illumination tapering of -12 dB at the edge of the reflector. The feed antennas can easily be scaled in frequency and operate in either linear polarisation (LP) or circular polarisation (CP).

In this work, only the horn illuminating reflector 2 is active and radiates in LP in the offset direction. The illuminated reflector has a diameter and focal length of 0.7 m and an offset of 0.49 m. The far-field of the complete geometry was computed in TICRA Tools using the MoM/MLFMM solver in ESTEAM and exported as a full sphere cut with a sampling spacing of 0.1° in θ and in ϕ, resulting in 6 481 800 sampling points in total. A normal distributed random noise level corresponding to a signal-to-noise ratio (SNR) of 60 dB was added to the data so synthesise a real measurement scenario.

A box enclosing the platform and the reflectors with the measures 4.1 m x 1.8 m x 3.6 m was used as RS. The re-

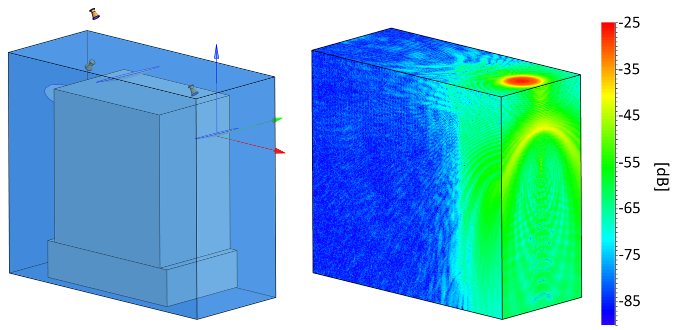

Fig. 3: Application case 1 with a box RS (left) and the magnitude of the reconstructed electric current density (right).

constructed currents on the RS were computed based on the total field from the feed and the platform with reflectors. The computational details of the reflector on platform source reconstruction case are presented in Table I. In summary, the problem consists of 3 229 688 higher order (HO) unknowns (equivalent to about 13 million Rao-Wilton-Glisson (RWG) unknowns), requires 60.2 GB random access memory (RAM) and finishes in a little over 4 h when analysed on a workstation computer with a Cascade Lake CPU with 32 physical cores. We stress that this is substantially lower than previously reported results in the literature, and in particular the RAM use is actually comparable to the RAM required for the forward problem, a remarkable conclusion.

The antenna geometry enclosed by the RS and the magnitude of the reconstructed equivalent electric current density are presented in Fig. 3. The centre feed horn is not enclosed by the RS since the scattering effect from this object on the radiated far-field was negligible. The reflector radiation is clearly visible and looks as expected in the reconstructed currents. A more detailed representation of the reconstructed currents is presented in Fig. 4, where the co-polarisation and cross-polarisation of the electric current density are viewed from the main beam direction of the reflector far-field.

To validate that the reconstructed currents are in fact the sought after unique physical currents, the scattered field from the platform and the reflectors was used as input for source reconstruction on the same RS that what was used for the total field. From this second set of reconstructed currents the root-mean-square error (RMSE) was computed in relation to the corresponding forward MoM currents computed in TICRA Tools ESTEAM. The RMSE of the electric current density is defined as

$$\mathrm{RMSE}_J = \sqrt{\frac{\sum_{i=1}^{N_{\mathrm{RMS}}} \left| \boldsymbol{J}_S^{\mathrm{rec}}(x_i, y_i, z_i) - \boldsymbol{J}_S^{\mathrm{ref}}(x_i, y_i, z_i) \right|^2}{\sum_{i=1}^{N_{\mathrm{RMS}}} \left| \boldsymbol{J}_S^{\mathrm{ref}}(x_i, y_i, z_i) \right|^2}}, \tag{15}$$

where $\boldsymbol{J}_S^{\mathrm{rec}}(x_i, y_i, z_i)$ and $\boldsymbol{J}_S^{\mathrm{ref}}(x_i, y_i, z_i)$ are the the reconstructed and reference MoM current densities evaluated at the points in space (x_i, y_i, z_i), and N_{RMS} is the number of equally spaced evaluation points on the RS. The definition in (15) was also used to evaluate the corresponding RMSE of the reconstructed magnetic current density. A worst-case RMSE of 6.6 % was computed, which is acceptable in relation to the requirements specified in the activity of RMSE $< 10\,\%$.

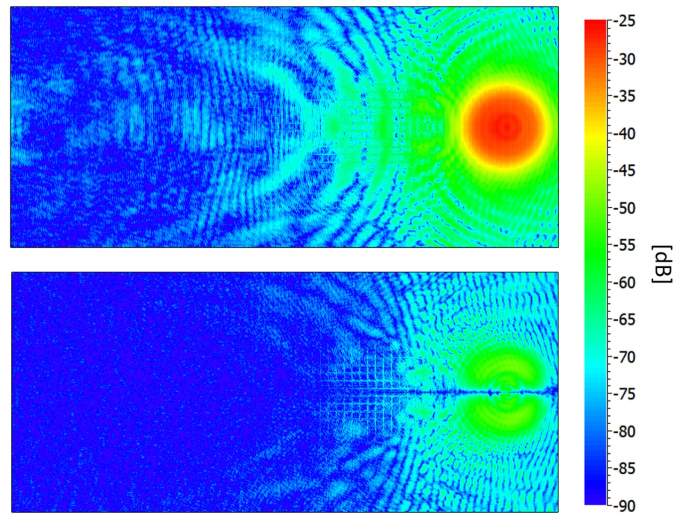

Fig. 4: Application case 1 reconstructed electric current density. The co-polarisation currents are presented at the top and the cross-polarisation currents at the bottom.

From the reconstructed currents the electric and magnetic fields can be computed anywhere in space outside of the RS. As an additional validation test, the reconstructed far-fields were computed and compared to the input far-field data provided to the algorithm. The far-field was computed with the sampling $\theta = [0, 180]^\circ$, $N_\theta = 1001$, $\phi = [0, 315]^\circ$, $N_\phi = 8$. The resulting far-field RMSE was $< 0.5\,\%$ which indicates that the input far-field was successfully reconstructed.

The synthetic measurement model in TICRA Tools enables the possibility to introduce different types of antenna defects to be detected. The feed and reflector of antenna 2 were translated 50 mm in the $-x$-direction, towards the platform, to achieve a reflector illumination blockage error, as is illustrated in Fig. 5. The enclosing box RS in Fig. 3 was re-used for the antenna defect source reconstruction problem, resulting in the same number of input data points and unknowns as in the nominal case. The reconstructed equivalent electric current density components computed from the total far-field of the defect antenna scenario are presented in Fig. 6. When comparing the reconstructed currents in Fig. 4 and in Fig. 6 it is seen that the blockage of the reflector illumination has an effect on the reconstructed currents, especially in the co-polar scattering from the rightmost side of the platform in Fig. 6.

B. Ice cloud imager 664 GHz feed horn

Next, the method was evaluated for source reconstruction of high frequency applications, where measurement data of a 664 GHz feed horn was used as input. The antenna had been measured by ESA at the European space research and technology centre (ESTEC) sub-mm wave scanner in support to the ice cloud imager instrument of the MetOp-SG program [17]. During the experimental characterisation of the antenna under test (AUT) an WR1.5 open ended waveguide (OEW)

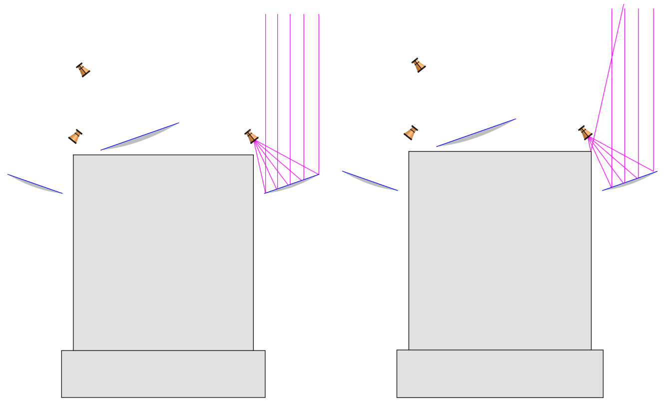

(a) (b)

Fig. 5: Nominal antenna setup (a) and a platform blockage error introduced to the radiating antenna (b).

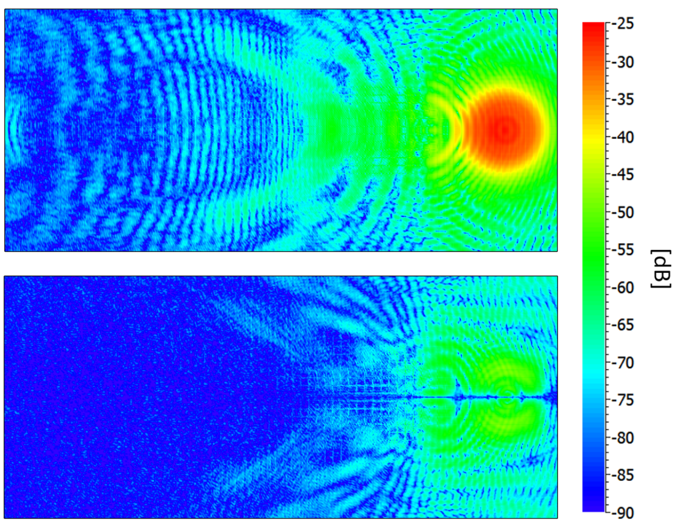

Fig. 6: Reconstructed electric current density where a reflector illumination blockage defect has been introduced. The co-polarisation currents are presented at the top and the cross-polarisation currents at the bottom.

with a conical shape for backscatter reduction was used as a probe. The co-polarisation and cross-polarisation near-fields were sampled over a planar scan surface of 20 mm x 20 mm located 2 mm in front of the AUT. Further details of the measurement campaign are presented in [17]. From the measured near-field data the far-field of the AUT was computed and provided to TICRA. Far-field data was only available in a truncated angular range in the forward hemisphere at the angles $\theta = [-75°, 75°]$. The sampling density of the provided far-field is 0.1° in θ and 22.5° in ϕ. Ideally, the data should have been sampled more densely in the ϕ-direction in order to fulfil the recommended sampling criterion for source reconstruction. To this end, a spherical wave expansion of the measured data was carried out as a preconditioning step to interpolate the measured data.

In order to carry out source reconstruction of the AUT knowledge of the physical envelope of the antenna is required.

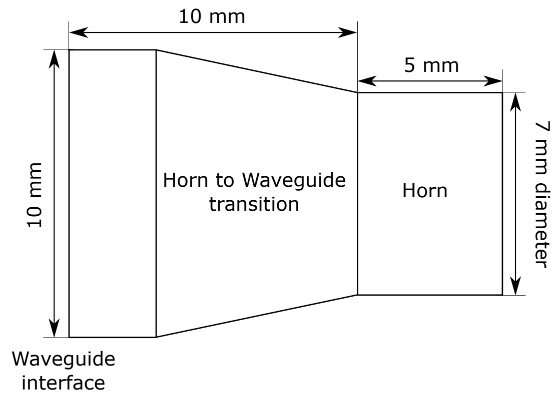

Fig. 7: Application case 2 envelope enclosing the AUT.

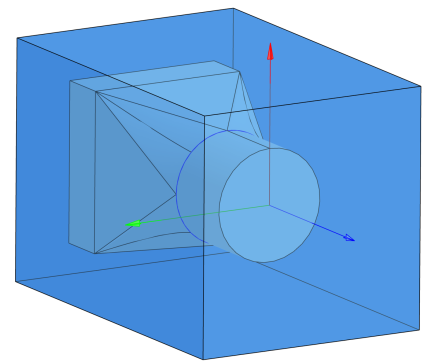

Fig. 8: Application case 2 AUT mock-up with the RS used in the source reconstruction analysis.

A sketch of the envelope of the AUT is presented in Fig. 7. A 15 mm x 15 mm x 22 mm box reconstruction surface was applied that encloses the AUT envelope, and provides some margin for AUT misalignments in the measurements, as is illustrated in Fig. 8. The computational details of the 664 GHz horn source reconstruction case are presented in Table I. The problem consists of 574 464 HO unknowns, it requires 6.0 GB of RAM and was computed in 44 minutes on the same 32 core computation machine as was used in Section IV-A. A much smaller computer could of course have been used in the analysis of the problem, with the main difference that the computation time would have been longer.

The two polarisation components of the reconstructed electric current density at the RS as seen from the AUT main beam direction are presented in Fig. 9. Since no prior information had been provided of the AUT radiation except for the far-field it was difficult to access the antenna performance solemnly based on the reconstructed currents. Nevertheless, the results indicate that the antenna performs as expected both in terms of the co-polarisation beam shape and the cross-polarisation levels and symmetry. In the same manner as for case 1, the reconstructed far-field was computed with the sampling $\theta = [0, 75]°$, $N_\theta = 1001$, $\phi = [0, 315]°$, $N_\phi = 8$. The resulting far-field RMSE was $< 0.3\,\%$ which shows that the input far-field had been successfully reconstructed by the source reconstruction solver.

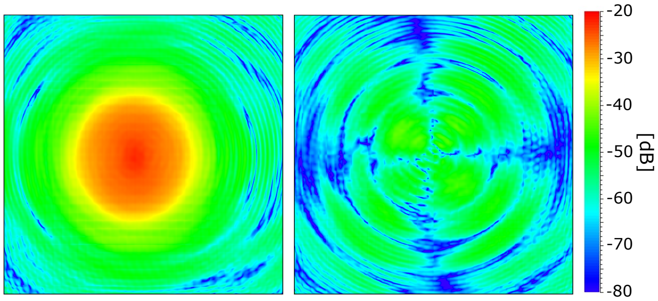

Fig. 9: Application case 2 reconstructed electric current density. The co-polarisation currents are presented to the left and the cross-polarisation currents to the right.

TABLE I: Analysis requirements of application cases 1 and 2, where the Calderón inverse 3D MoM method is compared to the previous state-of-the-art SCGLS inverse 3D MoM method.

Case	Solver	RS	Nbr. of unknowns	Memory req. (GB)	Comp. time (hh:mm)
1	Calderón	box	3 229 688	60	04:05
1	SCGLS	box	3 229 688	223 000	–:–
2	Calderón	box	574 464	6	00:44
2	SCGLS	box	574 464	6 660	–:–

C. Computational requirements

As a final step, source reconstruction of example case 1 in Section IV-A and example case 2 in Section IV-B were attempted using the 3D reconstruction method in DIATOOL 1.1, the most recent commercially available version of the software. The 3D reconstruction method in this software consists of a 3D MoM standard-form conjugate gradient least squares (SCGLS) solver, which represent the current state-of-the-art in terms of commercially available source reconstruction software. The main limitations of the SCGLS reconstruction method is the scaling of the memory requirements and simulation time in relation to the number of unknowns and the frequency of the AUT. For example, the simulation times scale with frequency as $\mathcal{O}(f^6)$. The values in Table I show that the high frequency horn example would require 6.66 TB of RAM to solve using SCGLS, and the reflector on platform example would require 223 TB of RAM. This comparison clearly displays the extreme acceleration that has been achieved in the new Calderón source reconstruction solver presented.

V. Conclusions

An extremely efficient implementation of a fast source reconstruction method for radiating structures on electrically large platforms has been presented for the first time. The implementation demonstrates drastic reductions in memory requirement and computation time in relation to current state-of-the-art source reconstruction solvers. In particular, the implementation is to the authors' knowledge the first published matrix-free source reconstruction method with $\mathcal{O}(N \log N)$ complexity. The effect of this complexity reduction in practice is so substantial that the memory requirements are comparable to that of solving the forward radiation problem, a substantial feat in any inverse solver implementation. Crucially, as we have demonstrated, these computational improvements come with no significant loss of accuracy.

References

[1] E. Jørgensen, P. Meincke, C. Cappellin, and M. Sabbadini, "Improved source reconstruction technique for antenna diagnostics,," in *Proceeedings of the 32nd ESA Antenna Workshop*, ESTEC, Noordwijk, The Netherlands, 2010.

[2] L. Foged, L. Scialacqua, F. Saccardi, J. A. Quijano, G. Vecchi, and M. Sabbadini, "Practical application of the equivalent source method as an antenna diagnostics tool [amta corner]," *IEEE Antennas and Propagation Magazine*, vol. 54, no. 5, pp. 243–249, 2012.

[3] E. Jørgensen, P. Meincke, and C. Cappellin, "Advanced processing of measured fields using field reconstruction techniques," in *European Conference on Antennas and Propagation*, 2011, pp. 3880–3884.

[4] J. L. Araque Quijano, L. Scialacqua, J. Zackrisson, L. J. Foged, M. Sabbadini, and G. Vecchi, "Suppression of undesired radiated fields based on equivalent currents reconstruction from measured data," *IEEE Antennas and Wireless Propagation Letters*, vol. 10, pp. 314–317, 2011.

[5] T. F. Eibert, E. Kilic, C. Lopez, R. A. M. Mauermayer, O. Neitz, and G. Schnattinger, "Electromagnetic Field Transformations for Measurements and Simulations (Invited Paper)," *Progress In Electromagnetics Research*, vol. 151, pp. 127–150, 2015.

[6] L. Scialacqua, L. J. Foged, F. Mioc, and F. Saccardi, "Link between measurement and simulation applied to antenna scattering and placement problems," in *2017 11th European Conference on Antennas and Propagation (EUCAP)*, 2017, pp. 2951–2955.

[7] B. Xu, Z. Ying, L. Scialacqua, A. Scannavini, L. J. Foged, T. Bolin, K. Zhao, S. He, and M. Gustafsson, "Radiation performance analysis of 28 ghz antennas integrated in 5g mobile terminal housing," *IEEE Access*, vol. 6, pp. 48 088–48 101, 2018.

[8] J. L. A. Quijano and G. Vecchi, "Field and source equivalence in source reconstruction on 3d surfaces," *Progress In Electromagnetics Research*, vol. 103, pp. 67–100, 2010.

[9] A. E. H. Love, "The Integration of the Equations of Propagation of Electric Waves," *Philosophical Transactions of the Royal Society A*, vol. 197, pp. 1–43, Sep. 1901.

[10] L. J. Foged, L. Scialacqua, F. Saccardi, J. L. A. Quijano, and G. Vecchi, "Application of the Dual-Equation Equivalent-Current Reconstruction to Electrically Large Structures by Fast Multipole Method Enhancement [AMTA Corner]," *IEEE Antennas and Propagation Magazine*, vol. 56, no. 5, pp. 264–273, Oct. 2014.

[11] T. F. Eibert and C. H. Schmidt, "Multilevel Fast Multipole Accelerated Inverse Equivalent Current Method Employing Rao–Wilton–Glisson Discretization of Electric and Magnetic Surface Currents," *IEEE Transactions on Antennas and Propagation*, vol. 57, no. 4, pp. 1178–1185, Mar. 2009.

[12] T. F. Eibert, D. Vojvodic, and T. B. Hansen, "Fast Inverse Equivalent Source Solutions With Directive Sources," *IEEE Transactions on Antennas and Propagation*, vol. 64, no. 11, pp. 4713–4724, Oct. 2016.

[13] E. Jørgensen, O. Kim, P. Meincke, and O. Breinbjerg, "Higher order hierarchical legendre basis functions in integral equation formulations applied to complex electromagnetic problems," in *IEEE AP-S International Symposium*, vol. 3A, Washington DC, USA, jul 2005, pp. 64–67.

[14] O. Borries, "Regularization Methods for Computation of Equivalent Sources," Technical University of Denmark, Tech. Rep., Nov. 2011.

[15] J. Kornprobst, R. A. M. Mauermayer, E. Kilic, and T. F. Eibert, "An Inverse Equivalent Surface Current Solver with Zero-Field Enforcement by Left-Hand Side Calderón Projection," in *European Conference on Antennas and Propagation*, Krakow, Jan. 2019, pp. 1–3.

[16] S. Schelkunoff, "Some equivalence theorems of electromagnetics and their application to radiation problems," *Bell System Technical Journal*, vol. 15, pp. 92–112, 1936.

[17] E. Saenz, M. Paquay, L. Rolo, E. van der Houwen, P. Radzik, P. de Maagt, U. Klein, G. Sonnabend, and D. M. Alvarez, "Measurements of the 664 ghz feed horn for the ici instrument of the metop-sg satellite," in *2017 International Symposium on Antennas and Propagation (ISAP)*. IEEE, 2017, pp. 1–2.